

Initial Mechanical Stability of Cementless Highly-Porous Titanium Tibial Components

Luke Amer¹, T. Brandon Stone², Christopher P. Warren³, Phillip Cornwell⁴, R. Michael Meneghini⁵

¹ University of Colorado – Boulder, Boulder, CO 80301

² Harding University, Searcy, AR 72143

³ University of Massachusetts – Lowell, Lowell, MA 01853

⁴ Department of Mechanical Engineering, Rose-Hulman Institute of Technology, Terre Haute, IN 47803

⁵ New England Musculoskeletal Institute, University of Connecticut Health Center, Farmington, CT 06030

Abstract

Cementless fixation in total knee replacement has seen limited use since reports of early failure surfaced in the late 1980s and early 1990s. However, the emergence of improved biomaterials, particularly porous titanium and tantalum, has led to a renewed interest in developing a cementless tibial component to enhance long-term survivorship of the implants. Cement is commonly used to mechanically fix orthopaedic implants, but represents a weak interface between the implant and the bone. The elimination of cement and application of these new biomaterials, which theoretically provide improved stability and ultimate osseointegration, would likely result in greater knee replacement success. Additionally, the removal of the cement from this procedure would eliminate the time needed for curing, thereby minimizing surgical durations and decreasing the risk of infection.

The purpose of this biomechanical study was twofold. The first goal was to assess whether vibration analysis techniques can be used to evaluate and characterize initial mechanical stability of cementless implants more accurately than the traditional method of micromotion determination, which employs linear variable differential transducers (LVDTs). The second goal was to perform an evaluative study to determine the comparative mechanical stability of five designs of cementless tibial components under mechanical loading designed to simulate *in vivo* forces. The test groups included a cemented Triathlon Keeled baseplate control group, three different 2-peg cementless baseplates with smooth-, mid-, and high- roughness, and a 4-peg cementless baseplate with mid-roughness.

1 Introduction

1.1 Background

Total knee arthroplasty (TKA) is a surgical procedure during which deteriorated or damaged bone and cartilage in the joints are replaced. During TKA a metal prosthesis implant is fixed to the bone and a plastic tibial insert is attached to this implant to replace the cartilage. Cementless fixation in TKA is not typically used because of its shortcomings relative to the traditional cemented designs and to the cementless designs with supplemental screw fixation. The determining factor governing the successful osseointegration of the bone and implant is the initial mechanical stability of the implant, which is the amount of relative micro-movement between the bone and the implant induced by the physiological joint loading shortly after the operation, before any biological process takes place [1-5].

In the past, cement and screw fixation techniques have provided assurance of the necessary initial mechanical stability [6-7]. Cementless designs have yet to outperform the well-established cemented tibial implants. There are many unanswered questions concerning the long-term reliability of the cementless knee implant. Proper designs which ensure the initial mechanical stability of the implant-bone interface and developments in highly porous materials could resolve some questions regarding cementless fixation [8-15]. Porous titanium may allow superior osseointegration of the bone into the implant.

The biomaterial implants were tested under loads which simulate *in vivo* (in the body) forces. Traditionally linear variable differential transducers (LVDTs) have been used to quantify the relative micromotion of the implant-bone interface during *in vitro* (out of the body) testing [16-19]. Piezoelectric (PZT) transducers have been studied extensively for use in structural health monitoring applications [20-22]. The mechanical impedance of the host structure is proportional to the electrical impedance of the PZT patch bonded to that structure. Measuring changes in the electrical impedance of the PZT patch can reveal changes in the mechanical impedance of a given structure and serve to detect the presence of damage [23].

1.2 Motivation

The primary motivation behind this study was to improve the longevity, reliability, and surgical duration of total knee replacement surgery by means of cementless fixation using porous metal technology. The current method utilizing cement to hold the tibial tray in place has been shown to be effective, with over a 90% implant survival rate after 10 years with many designs [15]. However, there are limitations inherent in using cemented tibial components. The difference in mechanical properties between the bone and cement create a weak interface, and the extended longevity of cement *in vivo* is uncertain [24]. Finally, knee replacement surgery with a cemented tibial fixation requires longer operating time to allow the cement to set and cure. A longer operating time translates to more exposure to microbial agents, which leads to an increased likelihood of infection in the patient.

It has been proposed that the utilization of porous metal baseplates would potentially overcome some of the aforementioned limitations concerning cemented implants [1-5]. Osseointegration of the patient's bone into the implant represents a biologically preferable and potentially longer lasting interface in comparison to cemented implants. Thus, by eliminating the cement interface and decreasing surgical times, a more robust tibial baseplate is envisioned. The crucial factor in the overall success of a cementless design is the initial mechanical stability. Determining a method to quickly and easily validate these new designs for this stability will aid in design development and ultimate application.

1.3 Purpose

The purpose of this biomechanical study was twofold: 1) to evaluate the micromotion of various cementless, porous-metal tibial baseplate designs in comparison to a proven, cemented control group, and 2) to determine if vibration measurements obtained using PZT patches are a valid alternative to using LVDTs which directly measure micromotion. There are numerous advantages to using PZTs rather than an array of LVDTs, which present difficulties with test fixture construction and experimental limitations associated with measuring relative displacements in all three orthogonal directions.

Five test groups were assessed under conditions which simulate *in vivo* loads. The LVDT outputs were continuously monitored during testing. A PZT was used as an individual, collocated actuator-sensor, mounted on the porous metal implant. Impedance spectra obtained using the PZT were taken before and after the preload was applied, after the cyclic loading, and finally while a static load equal to the maximum cyclic load was applied subsequent to the cyclic loading. Changes in the measured electrical impedance have been shown to be directly proportional to changes in the mechanical impedance of a structure [25].

2 EXPERIMENTAL PROCEDURES

2.1 Test Sample Preparation

Five groups of tibial baseplate implants were tested and are listed in Table 1 with their corresponding acronyms. A control group of a Triathlon Keeled baseplate was prepared using Simplex-P PMMA cement. The 2-peg designs had tapered 12.7 mm long pegs with

Acronym	Description
CEM	Cemented Triathlon Keeled control group
2PS	Cementless, 2-peg smooth, diffusion bonded particle sintered foam
2PM	Cementless, 2-peg mid roughness, selective laser melting
2PH	Cementless, 2-peg high roughness, selective laser melting
4PM	Cementless, 4-peg mid roughness, selective laser melting

a diameter of 9.5 mm at the baseplate. The 4-peg design had the same tapered peg with a diameter of 9.5 mm at the baseplate and with anterior pegs of length 9.5 mm and posterior pegs of length 5.7 mm. The 2-peg designs varied in surface roughness and were manufacturing process as follows. The 2-peg smooth diffusion bonded samples were particle sintered foam, PSF, which was diffusion bonded to the Titanium (Ti) baseplate and pegs. The other 2-peg designs, mid roughness and high roughness, were constructed using selective laser melting (SLM) on the underside of the baseplate. The peg roughness on these two designs was the same as the mid roughness SLM. The 4-peg surface was manufactured using the SLM method and was the same roughness as the 2-peg mid roughness SLM. The porosity of the PSF and SLM surfaces were identical at 63% and 62%, respectively, with a standard deviation of 4% as reported by Stryker Orthopedics. However, the rougher surface conditions were manufactured in such a way that resulted in less metal and more air at the surface.

The testing order was randomized to reduce systematic error. With the exception of the cemented control group specimens (prepared by Stryker), the rigid polyurethane foam tibial replicate sawbone specimens (Sawbones, Pacific Research Laboratories, Inc., Vashon, WA) were cut and drilled off-site by the manufacturer, Stryker Orthopedics. Figure 1 shows a 4-peg design and the predrilled holes. The implants were press-fit at the test facility with an impact tool supplied by Stryker after instruction from an orthopedic surgeon. The implants were implanted onsite to eliminate the vibration associated with transportation which could loosen or damage the implant or sawbone. One area of concern was that after being inserted, the edge of the implants came into contact with the hard shell of the sawbone models. The slight variation of this interface may have introduced some uncertainty due to the slight inconsistency of the interface among samples.



Figure 1. Sawbone model and implant.

2.2 Test Methodology and Remarks

2.2.1 LVDT Measurements

LVDTs were used to measure the micromotion between the sawbone and the implant. A rapid prototyped LVDT mount shown in Figure 2 was developed to ensure repeatability in the LVDT locations between test specimens. This mount screwed directly into the sawbone, fixing the location of six different LVDTs. Blocks were glued to the baseplate coplanar to the implant surface and aligned with the LVDT stems, resulting in six degrees of freedom in the measurement of the relative motion between the implant and the sawbone. LVDT measurements were sampled at a rate of 50 Hz during the cyclic loading. Figure 3 details the numbering convention of the setup.



Figure 2. Rapid-prototyped LVDT array.

2.2.2 Loading Conditions

Tibial baseplate samples were subjected to mechanical loading cycles designed to mimic the forces experienced by the tibio-femoral joint after TKA. The torsional, compressive, and shear forces experienced by the knee were considered prior to creating the test protocol. Normal compressive forces in the tibio-femoral joint range from 700 to 2200 N (1 to 3 times body weight), shear forces from 350 to 980 N, and torsion about the distal-proximal axis from 5 to 10 N-m. Originally, loads of 700 N compressive and 1000 N shear were chosen to mimic worst case conditions. The shear load was to be applied cyclically from 0 N to 1000 N at 0.1 Hz for 30 cycles. The minimum shear load applied was actually 50 N due to the MTS tensile testing machine's control system,

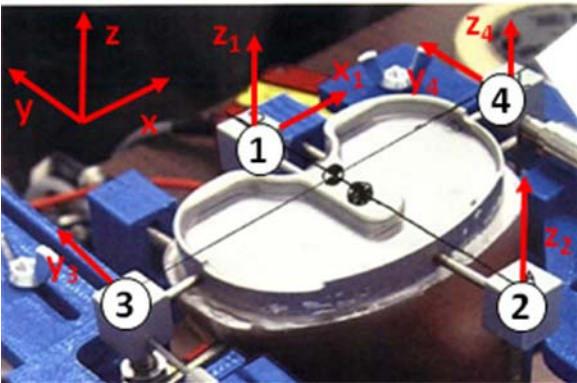


Figure 3. Direction for motion measurement and numbering convention for LVDT outputs.

which used the output force from the load cell for feedback. In addition, the femoral component was rotated 60° flexion about the medial-lateral axis and 6° (roughly twice what the joint normally sees) about the distal-proximal axis to induce torsion in the joint.

These loading conditions led to unrealistically large displacements in the first sample of the cemented control group. LVDT results for one of the samples from the cemented control group can be seen in Figure 4. In this figure the peaks correlate with the 1000 N load and the troughs with the 50 N shear load. The net motion detected by this LVDT was well over 200 μm , which is substantially larger than the clinically established threshold of 50 μm or less for these cemented implants.

Also noticeable was an upward and downward drift of the displacements in the z_1 and z_2 directions, respectively. Reviewing the displacement output of the MTS machine, it was determined that the drifting of the LVDT data

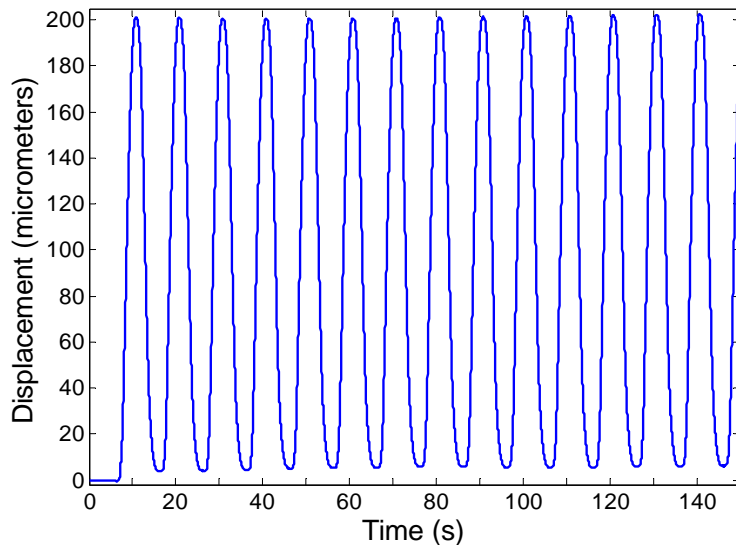


Figure 4. Displacement at LVDT 4, z_1 for 700 N compressive and 1000 N peak shear loads.

could possibly be attributed to viscoelastic deformation of the sawbone under the shear loading.

After thorough examination of the entire test structure, depicted in Figure 5, it was observed that the implant was lifting off along the posterior edge of the implant. During each cycle, a noticeable gap opened and closed between the implant and the sawbone along the posterior edge, near block 1. This lifting corresponds to large positive motion in z_1 and large negative motion in the z_2 direction. With 1000 N maximum shear load, a large moment was created at the interface of the implant and the sawbone causing lifting of the implant. The moment was caused by the reaction of the implant to the shear load applied at the plastic tibial insert by the femoral component. At this point, the 700 N compression and 1000 N shear applied loads were reconsidered. Previous

micromotion tests have illustrated that excessively large compressive loads drastically reduce the amount of measurable interfacial shear motion. Therefore, a relatively low compressive force of 700 N (roughly 1 times body weight) was selected. After adjusting the cyclic shear load to a peak of 350 N, the micromotion of a CEM implant measured by all 6 LVDTs fell below 15 μm . Thus, the sinusoidal shear force was reduced to a peak of 350 N with a minimum load of 50 N which was applied at a rate of 0.1 Hz for 30 cycles. This shear force is consistent with those used in previous micromotion studies [26]. These loading conditions became the protocol adopted for subsequent tests. Micromotion for all cemented samples was consistently less than 50 μm .

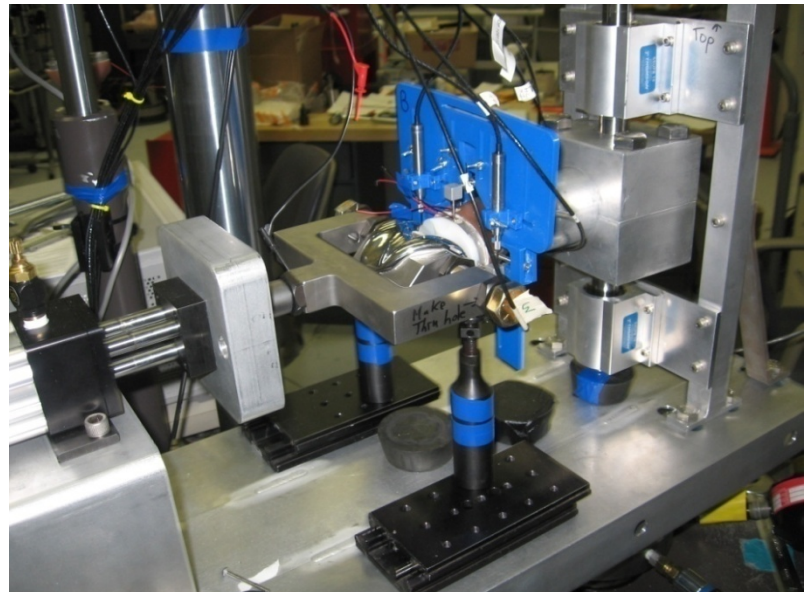


Figure 5. Experimental test apparatus.

2.2.3 PZT Measurements

The electrical impedance of a PZT patch is directly proportional to the mechanical impedance of the structure to which it is bonded. Changes in the mechanical impedance of the structure between pre- and post-loading states were used to detect interfacial micromotion. The testing protocol to compare the pre- and post-loading states was as follows. First, the pressure cylinder applied a 700 N compressive load to the femoral component at an angle of 60° flexion. Initially, impedance data from 40 Hz to 1.5 MHz was taken with the impedance analyzer. This served as the “baseline” measurement to determine the frequency range of interest for the structure. The impedance between 30 kHz and 350 kHz proved to be the most sensitive to changes in the sawbone-implant interface, so only this range was monitored in subsequent tests. The cyclic loading was then applied to the tibial component using an MTS machine and the compressive load of 700 N was maintained during the cyclic loading. After the 30 cycles were completed, impedance measurements were taken again. A static load of 350 N in the shear direction was then applied to the tibial component and impedance data was taken a third time during this static loading. The purpose of this step was to determine the impedance of the system at the maximum shear load and to compare it to the baseline impedance measurement of the system. After exploring three patch locations, it was determined that the most sensitive location was the location on the posterior medial side of the implant, labeled patch 1 in Figure 6.

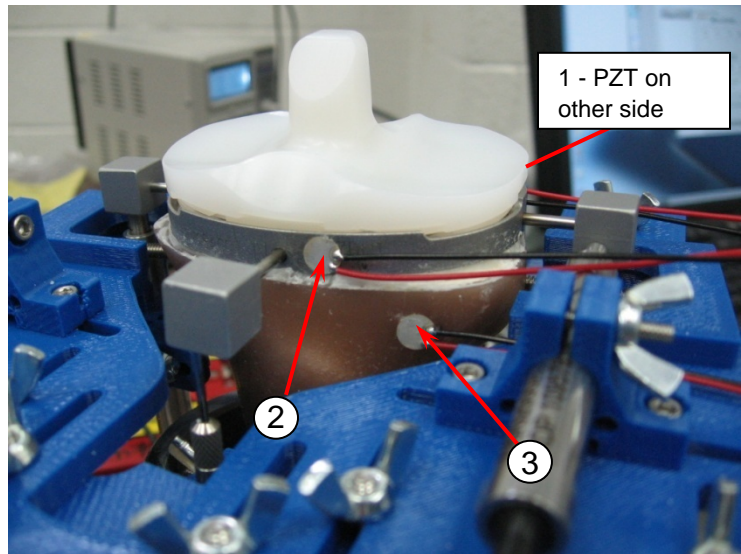


Figure 6. PZT patch locations are shown along with the polyethylene tibial insert.

3 EXPERIMENTAL RESULTS

3.1 LVDT Measurements

The LVDTs were in contact with blocks inserted into the implants as shown in Figure 2. Thus the motion measured was that of the block, not the implant itself. To transform the motion to the implant edge it was assumed that the implant could be treated as a rigid body and that all the displacements were small. A simple geometric transformation was used to translate the micromotion at the LVDT blocks to the motion of the implant. The motion in the z-direction at the medial and lateral posterior edges showed the greatest micromotion across all designs.

Figure 7 shows the average maximum implant motion at the medial posterior edge for each design group. As expected, the micromotion in the cemented design was substantially less than all cementless samples, shown in Table 2. The 2PS samples fall in a range that might allow for osseointegration of the bone into the implant.

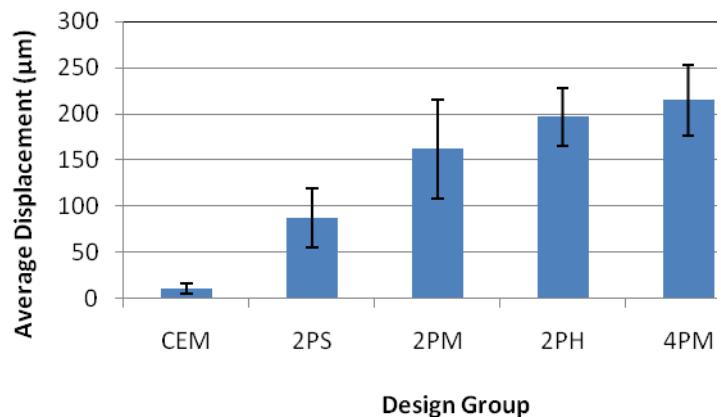


Figure 7. Average maximum implant motion at medial posterior edge (µm)

	CEM	2PS	2PM	2PH	4PM
Average (µm)	11	87	162	197	215
Standard Deviation (µm)	6	32	54	31	38

An ANOVA analysis, shown in Table 3, indicated that there was a statistical difference in the average maximum implant motion at the medial posterior edge between the cemented design and all the cementless designs with 95% confidence. Additionally, the 2PS design was found to be statistically different in average maximum micromotion than all the other designs tested.

Table 3: ANOVA Summary for Difference in z1 Micromotion at Posterior Medial of Implant ($\alpha = 0.05$)		
Groups Compared	P-Value	Reject Null Hypothesis ($\mu_1 = \mu_2$)
CEM-2PM	2.48E-4	Yes
CEM-2PS	7.32E-4	Yes
CEM-2PH	1.08E-6	Yes
CEM-4PM	2.55E-6	Yes
2PS-2PM	0.029	Yes
2PS-4PM	4.62E-4	Yes
2PS-2PH	5.93E-4	Yes
2PM-4PM	0.113	No
2PM-2PH	0.248	No
4PM-2PH	0.443	No

3.2 PZT Measurements

The impedance was determined at three different times: 1) after the 700 N compressive load was applied but before the 350 N cyclic shear load was applied, 2) after the 350 N cyclic loading, and 3) after a 350 N static load was applied. The 700 N compressive load was maintained during all three measurements. A typical result is shown in Figure 8. To characterize the change in impedance, the norm of the difference in the impedance was

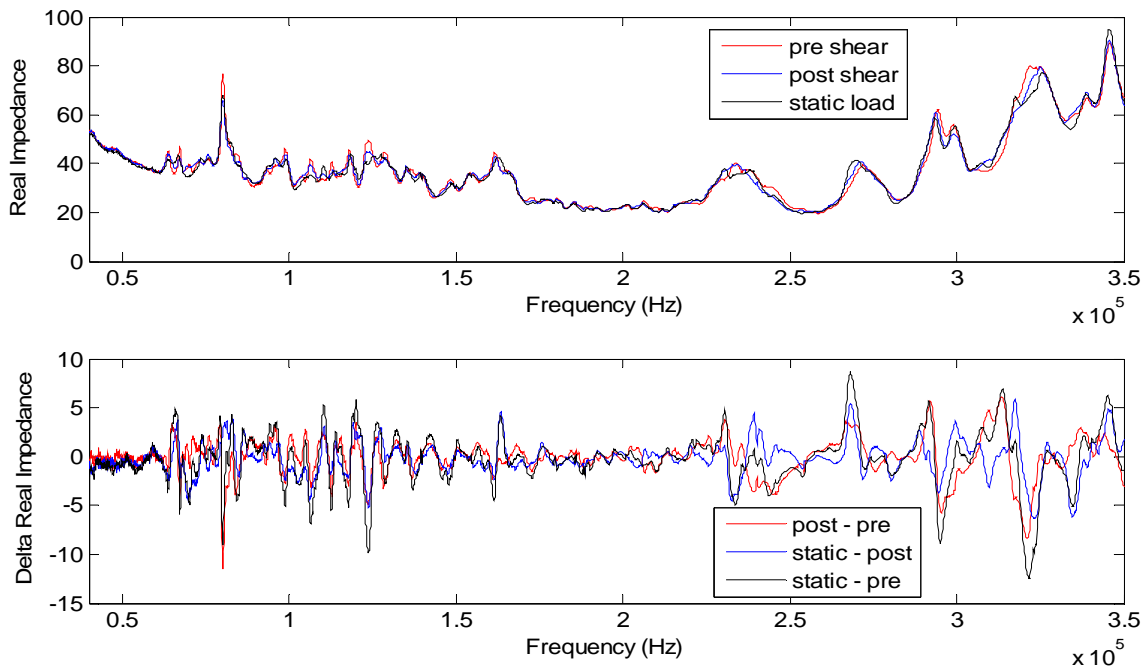


Figure 8. Typical impedance data. This set of data was for one of the two peg, high friction tests. The top plot is the impedance and the bottom plot is the difference in the impedance.

calculated using Eq. 1 where Z_{pre} is the magnitude of the real part of the impedance spectra after the 700 N compressive load was applied, Z_{static} is the magnitude of the real part of the impedance spectra after the 350 N static shear load was applied, and n is the number of data points in the frequency range being evaluated.

This metric was calculated using different frequency ranges. It is known that the resonant frequency of the PZT patch used typically lies in the 250 to 350 kHz range. Thus the impedance of the PZT patch around this frequency range was more susceptible to changes in the structure to which it was bonded. Initial attempts to correlate changes in the impedance traces before and after loading to the measured displacements at the LVDTs proved difficult with the inclusion of the 250 kHz and above frequency values. The impedance measurement turned out to be hypersensitive in this range, with the result that small variations in the system before and after loading dominated the change in impedance and this change was not necessarily due to micromotion at the interface. Therefore frequency values below 200 kHz were predominantly examined to define a metric relating micromotion measured by the LVDTs and the norm of the impedance difference. Furthermore, below 200 kHz, multiple frequency ranges were examined individually in comparison to the micromotion values.

There was a correlation between average maximum micromotion for a test group and the norm of the impedance difference when using a frequency range of 115–150 kHz as shown in Figure 9. The error bars are for one standard deviation. A plot of the average norm of the impedance difference in this frequency range for the various test groups is shown in Figure 10. The error bars correspond to one standard deviation. Using this same frequency range an ANOVA analysis was performed and the results are shown in Table 4. From this table it is clear that this metric shows a statistical difference between the cemented and the other groups as well as between the 2-peg smooth group and the two peg high-roughness and 4-peg mid-roughness groups. This result is consistent with the LVDT data translated to the implant motion in the z-direction. Thus within the frequency range of 115 to 150 kHz, it was found that the norm of the impedance was a useful metric to quantify micromotion when averaged over multiple replicates. However, there is a large degree of variability among specimens making it extremely difficult to find a strong correlation between micromotion and the change in impedance for the various trials of an individual implant (Figure 11).

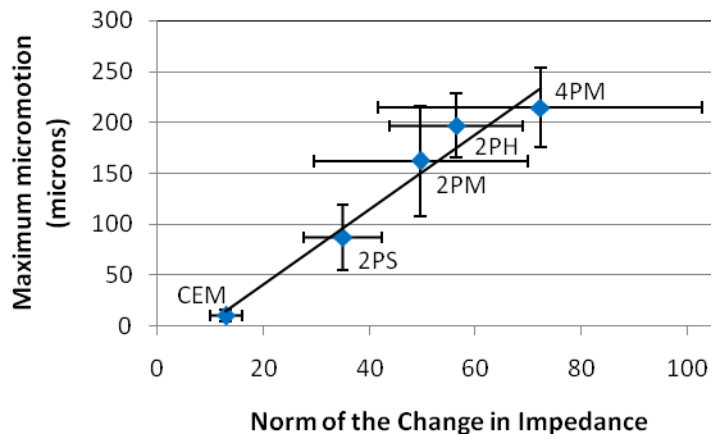


Figure 9 – Relationship between the motion at the center posterior in the z-direction and the norm of the difference in the impedance in the frequency range 115-150 kHz.

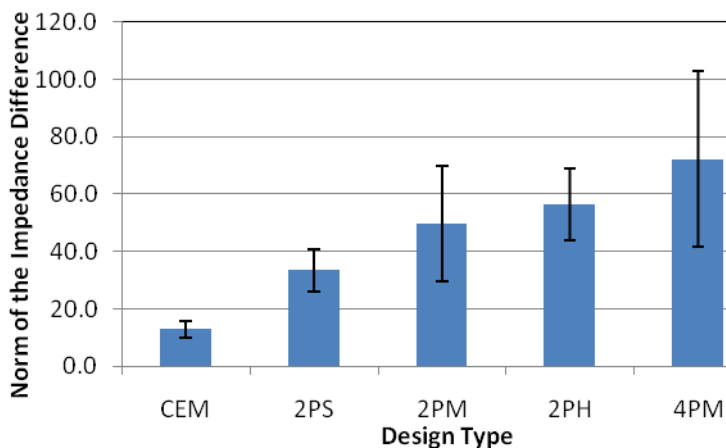


Figure 10 – Average norm of the difference in the impedance in the 115-150 kHz frequency range for the various test groups

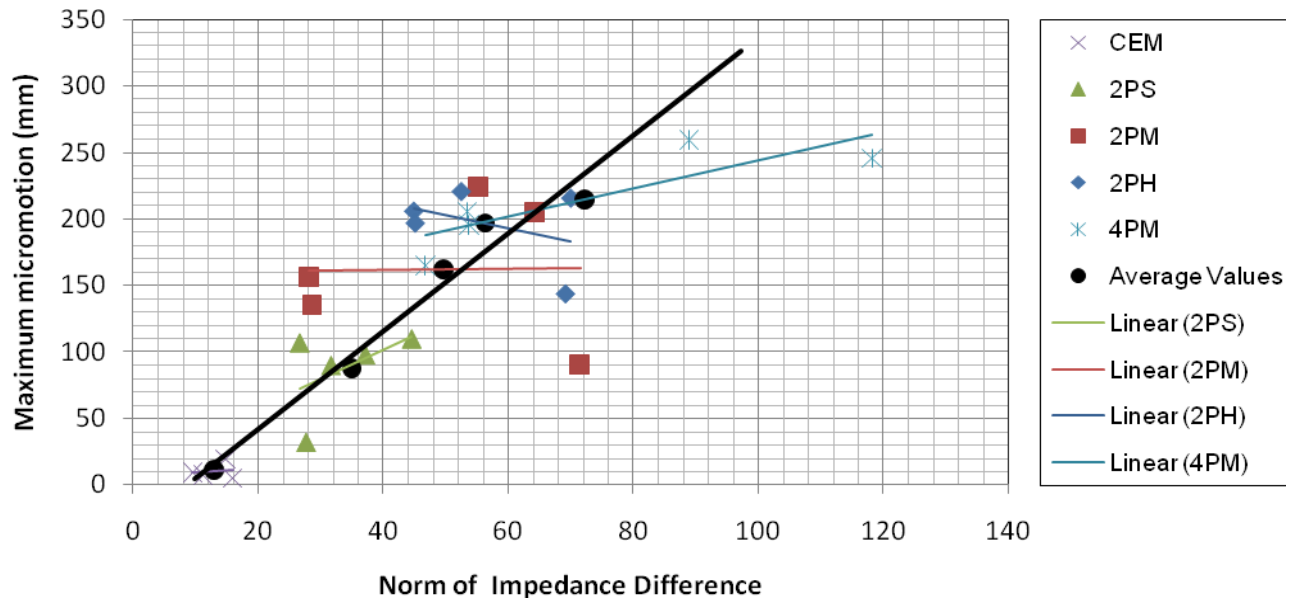


Figure 11 – Relationship between the motion at the posterior medial in the z-direction for all the samples and the norm of the impedance difference in the 115-150 kHz frequency range.

<u>Groups Compared</u>	<u>P-Value</u>	<u>Reject Null Hypothesis ($\mu_1 = \mu_2$)</u>
CEM-2PS	1.26E-03	Yes
CEM-2PM	9.16E-03	Yes
CEM-2PH	2.73E-04	Yes
CEM-4PM	6.54E-03	Yes
2PS-2PM	0.133	No
2PS-2PH	7.94E-03	Yes
2PS-4PM	0.025	Yes
2PM-2PH	0.543	No
2PM-4PM	0.204	No
2PH-4PM	0.312	No

This study has shown that in some cases the norm of the impedance difference can be used as a metric for identifying differences between designs provided a sufficient number of replicates are available. Unfortunately, the reliability of this correlation depended on what frequency range was used, and without the LVDT measurements it would not have been possible to know which frequency range to use. Therefore, even though the norm of the change of impedance can be correlated to the micromotion in some cases, and there was a frequency range where it distinguished between the test groups in the same way as

the LVDT measurements, there were significant shortcomings to this method. In particular, the change of impedance did not always correlate with micromotion for individual samples within a test group and the method requires using a particular frequency range which may change for different test samples or configurations.

Conclusions

The first goal of this study was to assess whether vibration based techniques using PZT transducers and impedance measurements can be used to evaluate and characterize initial mechanical stability of cementless tibial implants more accurately than the traditional LVDTs. It was determined that the vibration techniques are not robust enough to reliably determine micromotion and initial mechanical stability. Although it was possible to find a statistically significant correlation between changes in impedance and the micromotion, it was not possible to determine this correlation without LVDT micromotion data.

The second goal of this study was to evaluate the comparative mechanical stability of five designs of cementless tibial components under realistic loading conditions. It was determined that the design and surface conditions of the tibial implant had a statistically significant impact on the micromotion of the implant. The 2-peg smooth diffusion bonded implant was found to have statistically less micromotion than the other 2-peg and 4-peg designs. The reason for less micromotion of the 2-peg smooth design is not clear and will be a topic of further study [27,28]. The 2-peg designs of the implant were found to be superior to the 4-peg design. One possible explanation of this is that the pegs were shorter for the 4-peg design.

References

1. Bragdon, C.R., et al., *Differences in stiffness of the interface between a cementless porous implant and cancellous bone in vivo in dogs due to varying amounts of implant motion*. J Arthroplasty, 1996. **11**(8): pp. 945-51.
2. Engh, C.A., et al., *Quantification of implant micromotion, strain shielding, and bone resorption with porous-coated anatomic medullary locking femoral prostheses*. Clin Orthop Relat Res, 1992(285): pp. 13-29.
3. Pilliar, R.M., J.M. Lee, and C. Maniopoulos, *Observations on the effect of movement on bone ingrowth into porous-surfaced implants*. Clin Orthop Relat Res, 1986(208): pp. 108-113.
4. Soballe, K., et al., *Tissue ingrowth into titanium and hydroxyapatite-coated implants during stable and unstable mechanical conditions*. J Orthop Res, 1992. **10**(2): pp. 285-299.
5. M. Viceconti, G. Brusi, A. Pancanti, L. Cristofolini., *Primary Stability of an Anatomical Cementless Hip Stem: A Statistical Analysis*. J Biomechanics, 2006. **39**: pp. 1169-1179.
6. Kaiser, A.D. and L.A. Whiteside, *The effect of screws and pegs on the initial fixation stability of an uncemented unicondylar knee replacement*. Clin Orthop Relat Res, 1990(259): pp. 169-178.
7. Miura, H., et al., *Effects of screws and a sleeve on initial fixation in uncemented total knee tibial components*. Clin Orthop Relat Res, 1990(259): pp. 160-168.
8. Bobyn, J.D., et al., *Clinical validation of a structural porous tantalum biomaterial for adult reconstruction*. J Bone Joint Surg Am, 2004. **86-A Suppl 2**: pp. 123-129.
9. Bobyn, J.D., et al., *Characteristics of bone ingrowth and interface mechanics of a new porous tantalum biomaterial*. J Bone Joint Surg Br, 1999. **81**(5): pp. 907-914.
10. Christie, M.J., *Clinical applications of Trabecular Metal*. Am J Orthop, 2002. **31**(4): pp. 219-220.
11. Cohen, R., *A porous tantalum trabecular metal: basic science*. Am J Orthop, 2002. **31**(4): p. 216-217.
12. Findlay, D.M., et al., *The proliferation and phenotypic expression of human osteoblasts on tantalum metal*. Biomaterials, 2004. **25**(12): pp. 2215-2227.
13. Zardiackas, L.D., et al., *Structure, metallurgy, and mechanical properties of a porous tantalum foam*. J. Biomed Mater Res, 2001. **58**(2): pp. 180-187.
14. Zhang, Y., et al., *Interfacial frictional behavior: Cancellous bone, cortical bone and a novel porous tantalum biomaterial*. J Musc Res, 1999. **3**(4): pp. 245-251.

15. Lombardi AV Jr, Berasi CC, Berend KR., *Evolution of Tibial Fixation in Total Knee Arthroplasty*. The Journal of Arthroplasty, 2007. **22**(4): pp. 25-29.
16. Kraemer, W.J., I.J. Harrington, and T.C. Hearn, *Micromotion secondary to axial, torsional, and shear loads in two models of cementless tibial components*. J Arthroplasty, 1995. **10**(2): pp. 227-235.
17. Sala, M., M. Taylor, and K.E. Tanner, *Torsional stability of primary total knee replacement tibial prostheses: a biomechanical study in cadaveric bone*. J Arthroplasty, 1999. **14**(5): pp. 610-615.
18. Stern, S.H., R.D. Wills, and J.L. Gilbert, *The effect of tibial stem design on component micromotion in knee arthroplasty*. Clin Orthop Relat Res, 1997(345): pp. 44-52.
19. Yoshii, I., et al., *The effect of central stem and stem length on micromovement of the tibial tray*. J Arthroplasty, 1992. **7 Suppl**: pp. 433-438.
20. G. Park, H. Sohn, C. Farrar, and D. Inman. *Overview of Piezoelectric Impedance-Based Health Monitoring and Path Forward*. The Shock and Vibration Digest, 2003. **35**(6): pp. 451-463.
21. G. Park, C. Farrar, D. Inman. *4th International Workshop on Structural Health Monitoring, 2003*. pp. 1423-1430.
22. G. Park, J. Inman. "Impedance-Based Structural Health Monitoring." *Damage Prognosis For Aerospace, Civil and Mechanical Systems*. Ed. Daniel J Inman, Charles A Farrar, Vicente Lopez Junior, and Valder Steffen Junior. John Wiley and Sons: West Sussex, England, 2005., pp. 275-292.
23. G. Park, et al., *Piezoelectric Active Sensor Self-Diagnostics Using Electrical Admittance Measurements*. Journal of Vibrations and Acoustics, 2006(128): pp. 469-476.
24. S. Stern, R. Willis M.D., J. Gibbert PhD., *The Effect of Tibial Stem Design of Component Micromotion in Knee Arthroplasty*. Clinical Orthopedics and Related Research, 1997. **345**: pp. 44-52.
25. D. Abou-Trabi, M. Guthrie, H. Moore, P. Cornwell, A. Rosenberg MD., M. Meneghini MD., *Monitoring Femoral Component Insertion During Uncemented Total Hip Arthroplasty*. IMAC 2006.
26. W. Kraemer M.D., I. Harrington M.D., T. Hearn PhD., *Micromotion Secondary to Axial, torsional, and Shear Loads in Two Models of Cementless Tibial Components*. The Journal of Arthroplasty, 1995. **10**(2).
27. Meneghini, R.M. et al., *Novel Method for Testing Tibial Components Using Micromotion and Impedance Vibration Analysis*. Submitted to ORS 55th Annual Meeting, 2008.
28. Menighini, R., et al., *Effect of Surface Roughness on Mechanical Stability of Highly Porous Metal Cementless Tibial Implants*. Submitted to ORS 55th Annual Meeting, 2008.